Available online at www.sciencedirect.com
SCIENCE DIRECT®
Journal of Asian Earth Sciences 23 (2004) 705–713
Journal of Asian Earth Sciences
www.elsevier.com/locate/jseaes

Petrology of metabasites from the Terekta Complex as a constituent of ancient accretionary prism of Gorny Altai

N.I. Volkova[a,*], S.I. Stupakov[b], V.A. Simonov[b], Yu.V. Tikunov[b]

[a]*Institute of Mineralogy and Petrography, pr. Koptyuga 3, Novosibirsk 630090, Russia*
[b]*Institute of Geology, pr. Koptyuga 3, Novosibirsk 630090, Russia*

Abstract

The blueschist/greenshist Terekta Complex is the only blueschist locality known in the Russian Altai. The Terekta metabasites contain Na and Na–Ca amphibole, actinolite, phengite, epidote, albite, quartz, calcite, magnetite (or hematite). Depending on the amphibole composition, these rocks were subdivided into blueschist, transitional blueschist/greenschist and greenschist. Both blueschists and transitional blueschist/greenschists (glaucophane-bearing and winchite–actinolite schists) have compositions similar to alkaline basalts of oceanic islands, whereas the greenschists correspond to ocean-floor tholeiitic basalts, or MORB. Available geothermobarometry yielded the following estimates of metamorphic conditions: $T = 350–400$ °C and $P = 6–8$ kbar. The different mineral assemblages of the metabasites are believed to be a result of their different lithologies. The presence of matabasalts with ocean island basalt and MORB affinity, as well as the occurrence of layered metachert, marble, metagraywacke, and plates of serpentinized dunites, pyroxenites indicate that the complex was very likely a subduction-accretionary complex. The complex contains rocks of accretionary wedge, and fragments of oceanic crust which are regarded to be a remnant of an Early Paleozoic subduction zone in the Russian Altai.

Keywords: Gorny Altai; Terekta Complex; Accretionary wedge

1. Introduction

Phanerozoic accretionary events in Central Asia led to the formation of orogenic collage named Altaids (Sengör et al., 1993), or the Central Asian Orogenic Belt (Kovalenko et al., 1996; Jahn et al., 2000). The Altaids are composed of fragments of Palaeozoic and Mesozoic arcs, oceanic plateau, collisional complexes, which were successively accreted to the southern margin of the Siberian Craton. High-pressure/low-temperature metamorphic rocks are very rare in accretionary orogens like the Altaids and presumably originated at the early stages of development of the orogenic system. According to model by Sengör et al. (1993), such rocks are supposed not to occur there. Therefore, their occurrence may have a special geodynamic implication.

Except for glaucophane-bearing eclogite boudins within the Chagan–Uzun ophiolites from the Kurai zone (Buslov and Watanabe, 1996), the Terekta blueschist/greenschist Complex is the only locality of high-pressure metamorphic rocks, known in the Russian Altai (Dobretsov et al., 1972; Dobretsov et al., 1991; Duk, 1982; Duk, 1995). It is located in the central part of the Gorny Altai and comprises dismembered masses of metavolcanite, metagraywacke, metachert, marble, as well as of small plates and lens-shaped bodies of serpentinite and metadolerite (Dobretsov et al., 1991). All rocks were metamorphosed under blueschist and greenschist facies conditions. As blueschists are believed to mark the existence of former subduction zone, their recognition is important for geodynamic reconstruction, and documentation of their mineral assemblages is important for establishing $P–T$ conditions of subduction-zone metamorphism.

The purpose of this paper is to present the result of our detailed study on mineralogy and petrology of metabasites which are the principal constituent of the Terekta Complex. The results will be used to discuss the geodynamic implication of the Gorny Altai.

2. General geological setting

The Terekta Complex is located in the central part of Gorny Altai (Fig. 1, insert) and is a part of a terrain with

* Corresponding author.
E-mail address: nvolkova@uiggm.nsc.ru (N.I. Volkova).

1367-9120/03/$ - see front matter © 2003 Elsevier Ltd. All rights reserved.
doi:10.1016/S1367-9120(03)00127-5

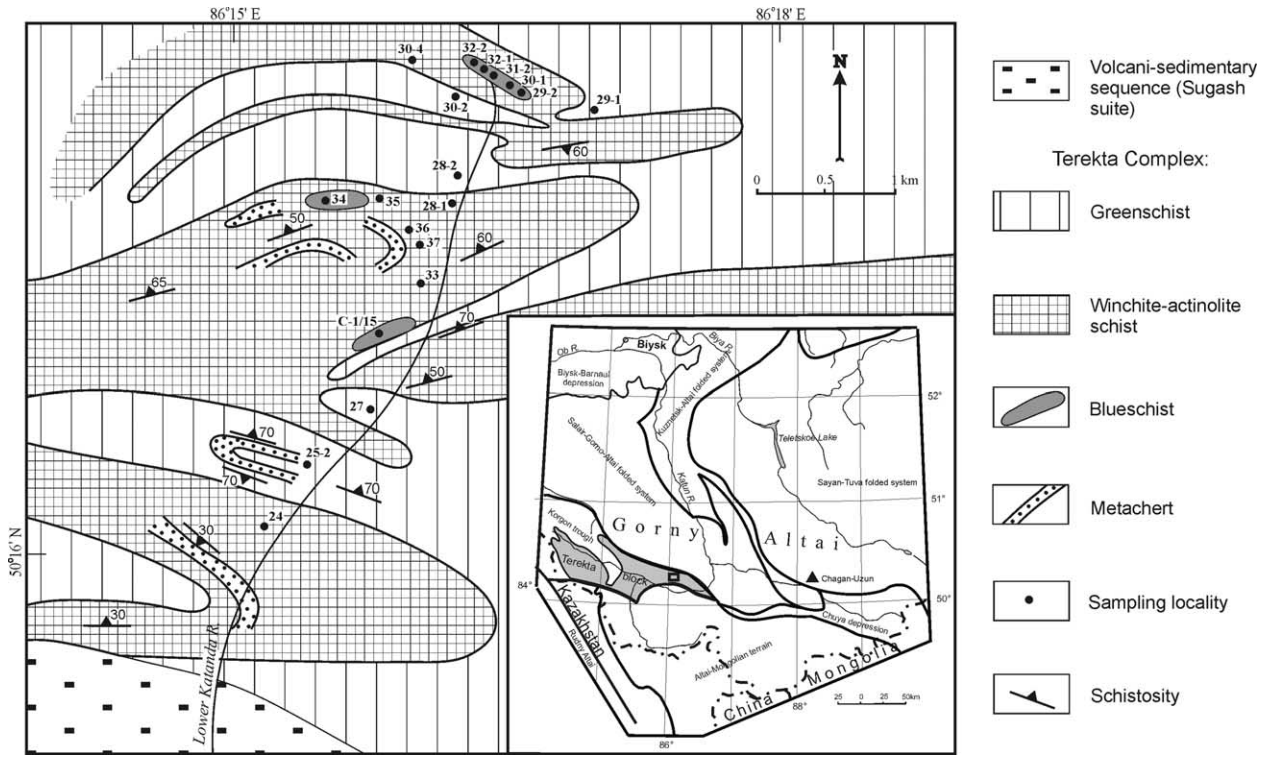

Fig. 1. Simplified geological map of the of the Lower Katanda River transect through the Uimon unit, the Terekta blueschist/greenschist complex (modified after Duk, 1982).

Middle Devonian imbricated structure, bounded by Upper Devonian–Early Carboniferous strike-slip faults (Dobretsov et al., 1991; Buslov et al., 2000). Apart from the Terekta Complex rocks, Dobretsov et al. (1991); Buslov (1998) distinguished the following tectonic units in the terrain: (1) Cambrian–Ordovician ophiolite plates described as foliated serpentinites with blocks of massive serpentinized dunites, pyroxenites, gabbro, and rodingites; (2) blocks or sheets of metamorphic rocks (schists, gneisses, amphibolites), formed under epidote–amphibolite facies at $T = 500–650$ °C, $P = 4–6$ kbar. These rocks are dated at $415 \pm 3, 418 \pm 3, 418 \pm 2$ Ma by the Ar–Ar method on an amphibole (Buslov, 1998); (3) Early Palaeozoic unmetamorphosed terrigene sediments.

The Terekta Complex is subdivided into two suites: the Uimon suite and the Terekta suite. The Uimon suite consists essentially of volcanic and volcaniclastic rocks, metamorphosed under transitional blueschist/greenschist facies conditions. Duk (1982, 1995) reported a K–Ar date of 1090 Ma on relict primary hornblende from actinolite schist. The date can be considered as an age of its protolith. Recent Sm–Nd whole-rock dating of metapelite rocks indicates model ages of 1160 to 1050 Ma for their protolith (Plotnikov et al., 2003). In addition, other K–Ar dates were reported for the Uimon metabasites: 570–600 Ma on a crossite from epidote–crossite schists, 600 Ma on a stilpnomelane, and 670–740 Ma on phengite and actinolite from actinolite schists (Duk, 1982, 1995). But Buslov (1998) reported new K–Ar dates of 455–400 Ma for the Uimon suite rocks (the dates were obtained in Okayama University, Japan).

The Terekta suite is composed partly of similar rocks, but differs by their metamorphic grade corresponding to greenschist facies, as well as by the predominance of metagraywackes and metacarbonate rocks.

The Terekta Complex is bordered on south by Cambrian–Ordovician volcanic-sedimentary series of the Sugash suite. The suite is composed of tuffs, tufogene sandstones, siliceous rocks, and calc-alkaline volcanic rocks of island arc affinity.

We would like to emphasize that the metabasites of the Terekta Complex differ substantially from the Chagan–Uzun eclogites in their appearance and petrological relation. Metamorphic rocks of the Chagan–Uzun ophiolite massif are represented by eclogites, amphibolites, and garnet amphibolites. They are massive rocks containing amphibole of barroisite–winchite series (Buslov and Watanabe, 1996) and were metamorphosed at higher $P–T$ conditions, as distinct from the Uimon blueschists. Moreover, these two localities of high-pressure rocks occupy different geological and structural position and are related to the different terranes. They differ also in their isotopic dates. The K–Ar dates on amphibole from the Chagan–Uzun eclogites is 535 ± 24 Ma, from garnet-free amphibolites is 523 ± 23 Ma, while the age of garnet amphibolites from crossing zones is 487 ± 22, 473 ± 13 Ma (Buslov and Watanabe, 1996; Buslov et al., 2001). Isotopic dating of eclogites from the Chagan–Uzun Massif using Ar–Ar

Table 1
Representative analyses of amphiboles from metabasites of the Terekta Complex

Sample	C-1/15				32-1				28-1			
Grain (MIneral)	7r (Gln)	1a (Gln)	9 (Gln)	7c (Gln)	31 (Gln)	23 (Gln)	35 (Gln)	22 (Gln)	72 (Win)	100 (Win)	99 (Win)	68 (Act)
SiO_2	55.49	54.25	54.84	56.88	55.79	56.48	56.96	56.93	51.34	53.05	53.30	55.02
TiO_2	0.01	0.04	0.05	0.01	0.05	0.02	0.03	0.02	0.08	0.09	0.01	0.00
Al_2O_3	8.47	8.32	7.98	7.67	6.69	8.77	8.86	8.48	4.36	3.44	3.42	1.63
FeO*	19.56	21.21	20.51	14.46	15.05	15.06	14.75	14.66	17.94	17.36	16.65	12.92
MnO	0.08	0.09	0.11	0.11	0.14	0.09	0.08	0.09	0.25	0.24	0.23	0.33
MgO	6.09	5.83	6.13	10.51	10.93	9.36	9.26	9.33	11.44	11.89	12.39	14.89
CaO	0.41	0.49	0.42	0.45	2.00	0.42	0.43	0.24	8.38	8.86	9.26	11.17
Na_2O	6.99	7.03	7.29	7.53	5.87	6.77	6.86	7.14	3.00	2.57	2.36	0.95
K_2O	0.07	0.03	0.03	0.02	0.02	0.02	0.04	0.03	0.19	0.17	0.17	0.08
Total	97.18	97.28	97.36	97.64	96.52	97.00	97.26	96.92	96.98	97.67	97.88	96.98
Si	7.93	7.79	7.87	7.89	7.83	7.86	7.91	7.95	7.52	7.70	7.70	7.93
Ti	<0.01	<0.01	0.01	<0.01	0.01	<0.01	<0.01	<0.01	0.01	0.01	0.01	0.00
Al (IV)	0.07	0.21	0.13	0.11	0.17	0.14	0.09	0.05	0.48	0.30	0.30	0.07
Al (VI)	1.36	1.20	1.22	1.14	0.94	1.30	1.36	1.35	0.27	0.29	0.28	0.21
Fe^{2+}	1.70	1.65	1.71	0.87	0.73	0.87	0.97	1.01	1.52	1.62	1.58	1.42
Fe^{3+}	0.63	0.90	0.75	0.81	1.04	0.88	0.74	0.70	0.68	0.49	0.43	0.13
Mn	0.01	0.01	0.01	0.01	0.02	0.01	0.01	0.01	0.03	0.03	0.03	0.04
Mg	1.30	1.25	1.31	2.17	2.28	1.94	1.92	1.94	2.50	2.57	2.67	3.20
Ca	0.06	0.08	0.07	0.07	0.30	0.06	0.07	0.04	1.31	1.38	1.43	1.72
Na	1.94	1.96	2.03	2.02	1.60	1.83	1.85	1.93	0.85	0.72	0.66	0.27
K	0.01	0.01	0.01	<0.01	<0.01	<0.01	0.01	0.01	0.04	0.03	0.03	0.01
$Mg/(Mg + Fe^{2+})$	0.43	0.43	0.43	0.71	0.76	0.69	0.66	0.66	0.62	0.61	0.63	0.69
Na (B site)	1.94	1.93	1.94	1.93	1.60	1.83	1.85	1.93	0.69	0.62	0.57	0.28

	30-4				25-2		
	121 (Win)	128 (Win)	125 (Act)	126 (Act)	37 (Act)	45 (Act)	62 (Act)
SiO_2	50.94	50.66	51.82	52.92	54.25	53.68	54.51
TiO_2	0.08	0.07	0.04	0.01	0.05	0.03	0.01
Al_2O_3	4.01	3.95	2.28	1.38	2.88	2.53	1.25
FeO*	20.9	20.52	19.58	17.77	15.56	15.03	12.6
MnO	0.23	0.21	0.25	0.18	0.28	0.28	0.29
MgO	9.74	9.84	11.09	12.27	12.45	12.94	15.89
CaO	9.20	9.35	10.09	11.47	11.25	11.24	11.73
Na_2O	2.10	2.07	1.49	0.64	0.98	0.98	0.50
K_2O	0.20	0.17	0.08	0.04	0.10	0.09	0.04
Total	97.40	96.84	96.71	96.68	97.79	96.80	96.82
Si	7.54	7.54	7.69	7.83	7.88	7.86	7.84
Ti	0.01	0.01	<0.01	<0.01	0.01	<0.01	<0.01
Al (IV)	0.46	0.46	0.31	0.17	0.12	0.14	0.16
Al (VI)	0.24	0.23	0.09	0.07	0.37	0.30	0.05
Fe^{2+}	1.92	1.95	1.86	1.94	1.89	1.83	1.16
Fe^{3+}	0.66	0.60	0.56	0.26	0.00	0.01	0.35
Mn	0.03	0.03	0.03	0.02	0.04	0.04	0.04
Mg	2.15	2.18	2.45	2.71	2.70	2.82	3.40
Ca	1.46	1.49	1.60	1.82	1.75	1.76	1.81
Na	0.60	0.60	0.43	0.18	0.28	0.28	0.14
K	0.04	0.03	0.02	0.01	0.02	0.02	0.01
$Mg/(Mg + Fe^{2+})$	0.53	0.53	0.57	0.58	0.59	0.61	0.75
Na (B site)	0.54	0.51	0.40	0.18	0.25	0.24	0.14

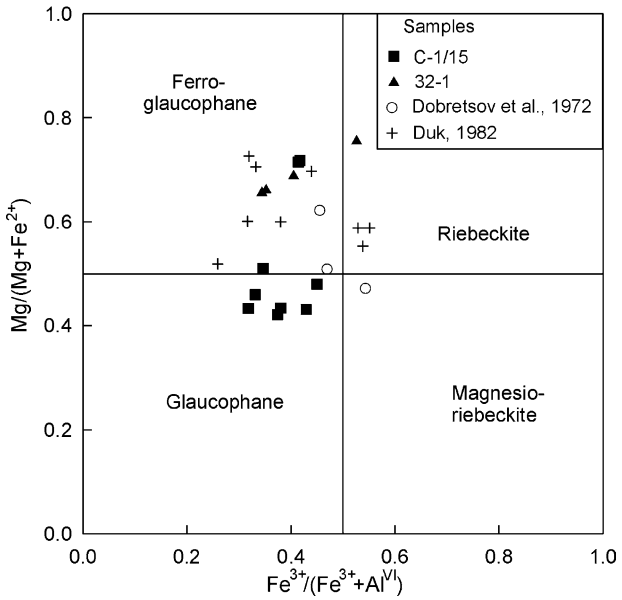

Fig. 2. Chemical composition of sodic amphibole from the Uimon suite of the Terekta Complex, Gorny Altai.

method on amphiboles gives an age of 636 ± 10, 627 ± 5 Ma for the eclogite facies metamorphism (Buslov, 1998; Buslov et al., 2001). So, we believe that there is no similarity between these two objects.

We have made a detailed sampling on the profile of the Uimon suite on the west bank of the Katun River along its tributary, the Lower Katanda River (Fig. 1). This profile of the Uimon suite is represented by a package of sheets, consisting mainly of metabasites which alternate with metagraywackes, metacherts with spessartine and piemontite, as well as thin lenses of marbles.

The Uimon metabasites are fine- to medium-grained schistose, or, more rarely, massive rocks. For most part, they consist of Na and Na–Ca amphibole, actinolite, phengite, epidote, albite, quartz, calcite; stilpnomelane and pumpellyite are rare. Titanite is present as an accessory phase in most samples. Hematite or magnetite, but not both, occur in trace amounts in some specimens. Such minerals as lawsonite, omphacite, aragonite, which are characteristic of HP/LT metamorphism, have not been found. The most common mineral assemblage is Amp + Ep + Chl + Phe + Ab + Qtz ± Mgt (Hem) ± Cal. Depending on amphibole composition, these rocks are subdivided into epidote blueschist (glaucophane-bearing), transitional blueschist–greenschist rock (with winchite and actinolite) and greenschist (only actinolite-bearing).

3. Mineral chemistry

3.1. Analytical techniques

All minerals were analysed with a 'Camebax-Micro' electron microprobe analyser in the United Institute of Geology, Geophysics and Mineralogy, Novosibirsk, Russia. An operating voltage of 20 kV, a beam current of 40 nA, a beam diameter of 2–3 μm, and a counting time of 10 s were employed for most analyses. Natural standards were used and the data were processed by the PAP routine. The determination error for all components was less than 2%. The Fe^{3+}/Fe^{2+} of amphibole is calculated assuming 13 total cations, exclusive of K, Na, and Ca (O = 23). The formula for stilpnomelane is normalised on the basis of 15 IV and VI cations and O = 23.813, identical to that used by Currie and Van Staal (1999).

Amphiboles. Sodic amphiboles are represented mainly by glaucophane and ferroglaucophane, Na–Ca amphiboles are winchite, rarely, barroisite, and calcic amphiboles are actinolite (Table 1), according to the IMA classification (Leake et al., 1997).

Small grains of sodic amphibole are usually unzoned. Occasionally, they have a slight zonation displayed in the paler colour, the increase of $Fe^{3+}/(Fe^{3+} + Al^{VI})$-ratio and, to a less extent, of Mg# number from core to rim. The zonation of blue amphiboles suggests that they grew with increasing temperature and decreasing pressure. Some of the apparent compositional variation within each sample may be due to the uncertainty in the Fe^{3+} calculation. However, the amphiboles of the selected samples generally fall within the Na-amphibole range (Fig. 2).

The Na_B content in Na–Ca amphiboles is 0.51–0.69, and Mg# number varies from 0.52 to 0.66 (Fig. 3, Table 1). It is worth noting that amphiboles with minimum $Mg_{\#}$-value (0.52–0.54) occur in stilpnomelane-bearing assemblages. The Na–Ca amphibole often coexists with actinolite having the same or somewhat lower $Mg_{\#}$-value. Some zoned amphibole grains with winchite core and actinolite rim were observed.

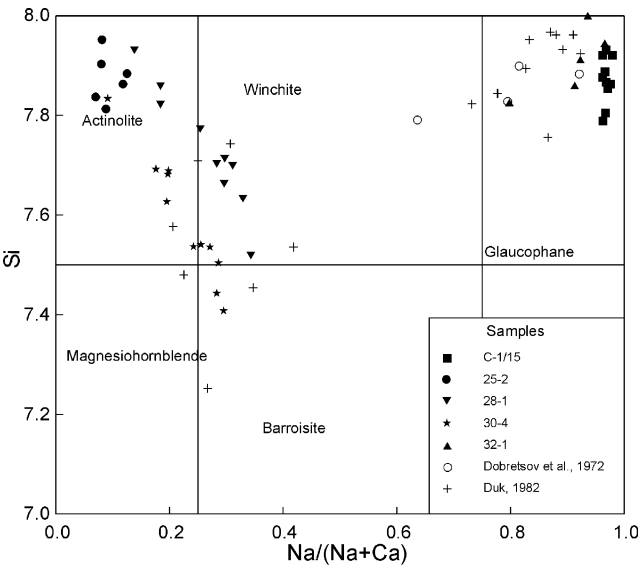

Fig. 3. Compositional plot of Si versus Na/(Na + Ca) for amphiboles from the Terekta Complex. (Classification scheme after Leake et al., 1997).

Table 2
Representative analyses of phengite, chlorite, epidote, albite and stilpnomelane

Sample	C-1/15					32-1					28-1							
Mineral	Phe	Phe	Chl	Chl	Ep	Phe	Phe	Phe	Ep	Chl	Phe	Phe	Phe	Ep	Ep	Chl	Chl	Ab
SiO_2	49.89	50.10	27.53	26.07	38.08	49.97	50.48	49.76	38.13	28.57	50.66	51.13	50.48	38.74	38.57	26.26	26.36	69.46
TiO_2	0.17	0.16	0.01	0.00	0.08	0.15	0.12	0.19	0.03	0.03	0.16	0.11	0.13	0.09	0.08	0.05	0.02	0.01
Al_2O_3	26.73	27.23	20.22	20.10	23.58	27.92	27.93	27.03	24.06	17.99	26.45	26.42	26.01	24.83	25.93	18.14	17.98	19.67
FeO(tot)	5.79	4.97	23.83	24.69	12.49	3.90	3.98	4.57	12.24	18.88	3.41	4.72	3.83	10.23	9.23	27.08	26.81	0.06
MnO	0.00	0.03	0.40	0.43	0.26	0.00	0.01	0.01	0.23	0.48	0.03	0.02	0.04	0.20	0.25	0.39	0.38	0.01
MgO	2.28	2.17	16.02	16.89	0.03	2.83	2.66	2.85	0.07	22.43	3.39	3.26	3.39	0.03	0.03	15.58	15.30	0.01
CaO	0.00	0.00	0.00	0.00	23.43	0.02	0.01	0.02	21.99	0.12	0.08	0.03	0.05	23.37	23.25	0.08	0.08	0.06
Na_2O	0.44	0.45	0.13	0.03	0.05	0.39	0.36	0.33	0.07	0.04	0.27	0.14	0.24	0.03	0.04	0.04	0.05	10.75
K_2O	10.61	10.67	0.04	0.01	0.03	10.17	10.09	10.22	0.26	0.02	10.2	9.95	10.37	0.01	0.00	0.06	0.03	0.04
Total	95.91	95.78	88.18	88.22	98.03	95.35	95.64	94.98	97.07	88.55	94.64	95.77	94.53	97.54	97.39	87.68	87.02	100.05
	O = 11	O = 11	O = 14	O = 14	O = 12.5	O = 11	O = 11	O = 11	O = 12.5	O = 14	O = 11	O = 11	O = 11	O = 12.5	O = 12.5	O = 14	O = 14	O = 8
Si	3.362	3.376	2.852	2.715	2.994	3.341	3.363	3.351	3.012	2.867	3.410	3.392	3.411	3.036	3.016	2.790	2.824	3.015
Ti	0.009	0.008	0.001	0.000	0.005	0.008	0.006	0.010	0.002	0.002	0.008	0.005	0.006	0.006	0.004	0.004	0.002	0.000
Al	2.124	2.163	2.470	2.468	2.185	2.201	2.194	2.146	2.241	2.128	2.099	2.067	2.072	2.294	2.390	2.272	2.271	1.007
Fe^{3+}	0.065	0.000	0.000	0.110	0.809	0.081	0.061	0.110	0.801	0.143	0.043	0.174	0.060	0.650	0.598	0.157	0.094	0.002
Fe^{2+}	0.261	0.28	2.065	2.040	0.013	0.137	0.161	0.147	0.008	1.442	0.148	0.088	0.157	0.021	0.006	2.149	2.308	0.000
Mn	0.000	0.002	0.035	0.038	0.017	0.000	0.000	0.001	0.015	0.041	0.001	0.001	0.002	0.013	0.016	0.035	0.035	0.000
Mg	0.229	0.218	2.474	2.621	0.004	0.282	0.264	0.286	0.008	3.355	0.340	0.322	0.341	0.003	0.004	2.467	2.443	0.001
Ca	0.000	0.000	0.000	0.000	1.974	0.001	0.001	0.001	1.861	0.013	0.005	0.002	0.003	1.962	1.948	0.009	0.009	0.003
Na	0.057	0.058	0.026	0.006	0.007	0.050	0.047	0.043	0.01	0.007	0.035	0.018	0.031	0.005	0.007	0.009	0.011	0.905
K	0.913	0.918	0.005	0.002	0.003	0.868	0.859	0.879	0.026	0.002	0.877	0.843	0.895	0.001	0.000	0.008	0.003	0.002
Sum	7.020	7.023	9.927	10.000	8.010	6.970	6.956	6.973	7.984	10.000	6.967	6.912	6.980	7.990	7.989	10.000	10.000	4.935

	30-4							25-2				
	Ep	Ep	Stp	Stp	Chl	Chl	Ab	Ep	Ep	Chl	Chl	Ab
SiO_2	38.43	37.63	44.51	45.05	25.41	25.36	68.54	39.31	39.07	26.08	26.50	69.74
TiO_2	0.09	0.05	0.02	0.01	0.04	0.04	0.01	0.08	0.07	0.01	0.04	0.01
Al_2O_3	25.74	22.92	6.22	6.12	19.08	19.10	20.03	27.27	26.76	19.76	19.51	19.67
FeO(tot)	9.87	12.96	29.04	29.15	31.62	31.86	0.13	8.10	8.18	26.20	25.66	0.06
MnO	0.17	0.16	0.71	0.76	0.20	0.18	0.01	0.20	0.21	0.38	0.33	0.00
MgO	0.04	0.04	5.48	5.31	11.43	11.18	0.01	0.04	0.22	13.81	14.32	0.01
CaO	23.39	23.10	0.46	0.41	0.08	0.06	0.04	22.78	23.47	0.11	0.08	0.04
Na_2O	0.00	0.02	0.12	0.02	0.00	0.05	11.38	0.07	0.04	0.05	0.02	10.69
K_2O	0.00	0.00	1.26	0.95	0.01	0.01	0.04	0.01	0.01	0.02	0.003	0.04
Total	97.72	96.88	87.82	87.78	87.86	87.84	100.26	97.87	98.03	86.41	86.46	100.26
	O = 12.5	O = 12.5	O = 23.81	O = 23.81	O = 14	O = 14	O = 8	O = 12.5	O = 12.5	O = 14	O = 14	O = 8

(*continued on next page*)

Table 2 (*continued*)

Sample	30-4							25-2					
Mineral	Ep	Ep	Stp	Stp	Chl	Chl	Ab	Ep	Ep	Chl	Chl	Ab	
Si	3.000	2.995	7.867	7.935	2.772	2.770	2.983	3.037	3.026	2.806	2.838	3.019	
Ti	0.005	0.003	0.003	0.002	0.003	0.004	0.000	0.005	0.004	0.001	0.003	0.000	
Al	2.369	2.151	1.295	1.270	2.454	2.460	1.028	2.484	2.444	2.507	2.463	1.004	
Fe^{3+}	0.638	0.854	0.091	0.109	0.000	0.004	0.000	0.518	0.507	0.000	0.000	0.002	
Fe^{2+}	0.006	0.009	4.194	4.178	2.885	2.907	0.005	0.005	0.023	2.358	2.298	0.000	
Mn	0.011	0.011	0.106	0.114	0.018	0.017	0.000	0.013	0.013	0.034	0.030	0.000	
Mg	0.004	0.004	1.443	1.393	1.858	1.820	0.001	0.005	0.026	2.215	2.285	0.001	
Ca	1.957	1.970	0.086	0.077	0.009	0.007	0.002	1.886	1.948	0.012	0.009	0.002	
Na	0.000	0.004	0.041	0.006	0.000	0.011	0.960	0.010	0.005	0.010	0.004	0.897	
K	0.000	0.000	0.284	0.213	0.001	0.001	0.002	0.001	0.001	0.003	0.000	0.002	
Sum	7.990	8.001	15.410	15.297	10.000	10.000	4.981	7.963	7.998	9.946	9.930	4.927	

Ca amphibole corresponds in composition to actinolite. It occurs together with winchite in transitional blueschist/-greenschists, as well as the only amphibole in greenschists. Actinolite from greenschists is characterized by a lower Na content and a wider range of Mg# values (0.58–0.75), as compared with actinolite from winchite–actinolite schists (Table 1, Fig. 3).

Phengites contain appreciable amounts of celadonite component (Table 2), with Si varying from 3.30 to 3.39 p.f.u (O = 11). There is no regular zonation in most phengites. However, compositional scanning of some phengite crystals in glaucophane-bearing schists indicate a decrease of Al and an increase of Si and Fe from core to rim. Rarely, a slight decrease of Si from core to rim was found. *Chlorite* occurs as subhedral crystals arranged parallel to the schistosity. It is present in most samples and displays anomalous brown interference colours. Its Mg# number varies from 39 to 56% depending on rock composition. Chlorite tend to decrease in Mg# number from blueschist through transitional blueschist/greenschist to greenschist (Table 2). Chlorite with the minimum Mg# value (39%) occurs in stilpnomelane-bearing assemblages. *Epidote* occurs as subhedral to euhedral, pale yellow-green grains. Pistacite content varies from 32.2 to 17.0%, with the minimum values (17.0–20.0%) in greenschists. All analysed *plagioclase* grains are nearly pure albite, containing less than 1 mol% anorthite. *Stilpnomelane* occurs only in a few samples as radiating tabular brown-coloured grains, usually cutting the schistosity and is represented by ferrostilpnomelane (Table 2).

4. Estimation of temperatures and pressures

It has been known that variations in mineral compositions can be due to P–T conditions or bulk rock composition, or both the factors. Our whole-rock chemistry data (Table 3) of the Uimon metabasites show that the three rock types display significant differences in TiO_2, MgO, Na_2O, K_2O, and P_2O_5 contents. The differences are also consistent with earlier published major-oxide and trace-element analyses (Duk, 1982; Kuznetsova, 1985). In the Zr–Nb–Y diagram of Meschede (1986), the blueschists and transitional blueschists/greenschists (winchite–actinolite-bearing schists) fall in the field of within-plate basalts, while the greenschists fall within the fields of E-type and N-type MORB (Fig. 4). These data suggest that the blueschists are similar in composition to alkaline basalts of oceanic islands, whereas greenschists correspond to tholeiite basalts of MORB type.

It should be noted that Mg-rich layers did not develop sodic amphibole. In their turn, the examined glaucophane-bearing schists usually do not display any features of retrogressive metamorphic overprint. So, we can conclude that the mineralogical variation between interlayered

Table 3
Chemical composition of metabasites from the Terekta Complex

	SiO_2	TiO_2	Al_2O_3	Fe_2O_3(tot)	MnO	MgO	CaO	Na_2O	K_2O	P_2O_5	LOI	Total
Blueschist												
29-2	45.24	3.36	14.23	15.80	0.22	5.42	6.65	3.18	1.88	0.43	3.04	99.45
30-1	46.10	3.13	13.37	15.20	0.24	5.57	9.07	2.36	1.44	0.49	1.81	98.77
31-2	46.00	2.72	16.11	14.91	0.27	5.43	4.81	3.49	1.89	0.47	3.02	99.11
32-1	45.85	2.24	15.28	11.95	0.22	6.56	10.42	2.32	1.66	0.33	2.67	99.50
32-2	46.73	3.47	14.88	13.83	0.17	4.40	6.31	3.64	3.28	0.58	2.83	100.12
34	42.39	2.65	14.59	15.42	0.23	6.32	12.06	3.67	0.98	0.36	1.68	100.34
Average	45.39	**2.93**	14.74	14.52	0.23	**5.62**	8.22	**3.11**	**1.86**	**0.44**	2.48	99.55
Transitional blueschist/greenschist												
24	45.60	1.46	11.71	11.59	0.51	6.71	11.06	4.62	0.61	0.25	3.25	100.04
28-1	46.92	2.05	14.05	11.77	0.22	7.16	10.66	3.13	1.07	0.30	2.97	100.30
33	45.48	2.15	14.57	12.77	0.22	6.41	10.71	3.63	0.72	0.33	2.49	99.48
35	48.08	1.90	14.90	11.62	0.18	6.70	8.41	4.39	0.69	0.23	2.41	99.51
36	46.80	1.84	14.69	11.66	0.21	6.82	9.05	5.70	0.55	0.26	2.26	99.84
37	45.13	1.91	14.71	12.46	0.23	8.45	9.59	4.13	0.24	0.25	2.78	99.88
30-4	46.08	1.80	9.88	14.95	0.22	6.92	10.35	3.16	0.19	0.15	5.42	99.12
Average	46.25	**1.87**	13.93	12.40	0.25	**7.02**	9.98	**4.11**	**0.58**	**0.25**	3.08	99.72
Greenschist												
25-2	46.34	1.26	13.56	12.46	0.23	8.60	12.49	2.64	0.04	0.11	2.31	100.04
27	45.45	1.86	13.23	15.54	0.25	8.54	8.88	2.34	0.06	0.16	3.17	99.49
28-2	45.71	1.56	15.18	10.39	0.18	7.73	14.27	1.97	0.34	0.20	2.83	100.36
29-1	46.80	1.64	13.53	13.90	0.25	7.86	11.37	2.33	0.03	0.13	2.27	100.12
30-2	47.26	0.80	14.18	10.38	0.20	9.51	13.30	1.97	0.07	0.05	2.21	99.93
Average	46.31	**1.42**	13.94	12.53	0.22	**8.45**	12.06	**2.25**	**0.11**	**0.13**	2.56	99.98

The average contents of oxides showing statistically significant differences between the three rock types, are bolded.

blueschists and greenschists are probably related to the bulk rock chemistry.

The P–T conditions of metamorphism can only be estimated roughly, because independent geothermobarometers are almost not available for the studied rocks. The lack of some index minerals helps to constrain the P–T conditions of the investigated rocks. The absence of sodic pyroxene (omphacite or jadeite) indicates that the complex did not undergo pressures higher than 9–10 kbar (El-Shazly, 1994). The absence of metamorphic hornblende indicates that temperatures did not exceed ~500 °C (Winkler, 1976). In addition, the lack of oligoclase and anorthite indicates that metamorphic temperatures were below 450–550 °C (Maruyama et al., 1983).

P–T conditions of metamorphism are estimated to be 350–400 °C and 6–8 kbar using the (Na–Ca) amphibole–albite–chlorite–epidote–quartz geothermobarometer (Triboulet, 1992). Estimates of uncertainty are difficult to assess, but are no more than ± 80 °C and 1.5 kbar. Attempts at calculating the P–T conditions of metamorphism using the THERMOCALC program (Holland and Powell, 1998) led to the close agreement of the pressure estimates and overestimated temperatures (~400–450 °C).

The petrogenetic grid calculated by Evans (1990) for low-grade mafic rocks (Fig. 5) shows different P–T fields for the glaucophane–epidote stability field, depending on the chemistry of glaucophane (hence, bulk-rock chemistry). We used two types of the grid by Evans (1990) in accordance with mineral chemistry and mineral assemblages for blueschists (Fig. 5a) as for more ferrous rocks, and for greenschists (Fig. 5b) as for more magnesian rocks. The grids shows that the glaucophane–epidote stability field is considerably reduced for magnesian compositions. This is fully consistent with our observations that glaucophane

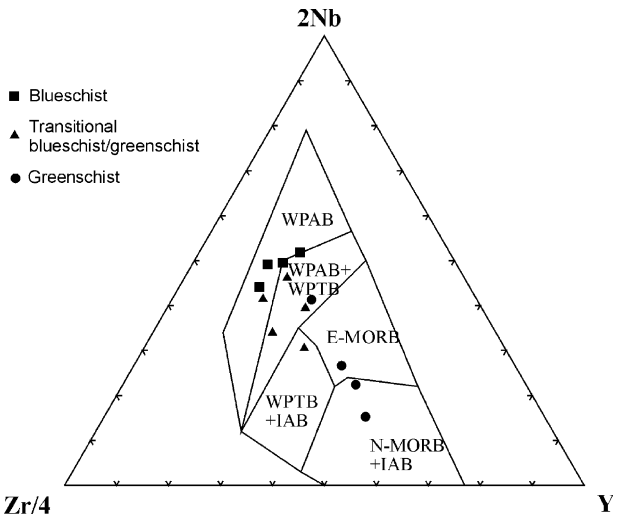

Fig. 4. Zr–Nb–Y ternary diagram for the Uimon metabasites from the Terekta Complex. The trace element analyses were taken from Kuznetsova (1985). Fields based on Meschede (1986): WPAB, within-plate alkali basalts; WPTB, within-plate tholeiitic basalts; E-MORB, basalts from plume-influenced regions (P-type MORB); IAB, island arc basalts; N-type MORB, 'normal' mid-ocean basalts.

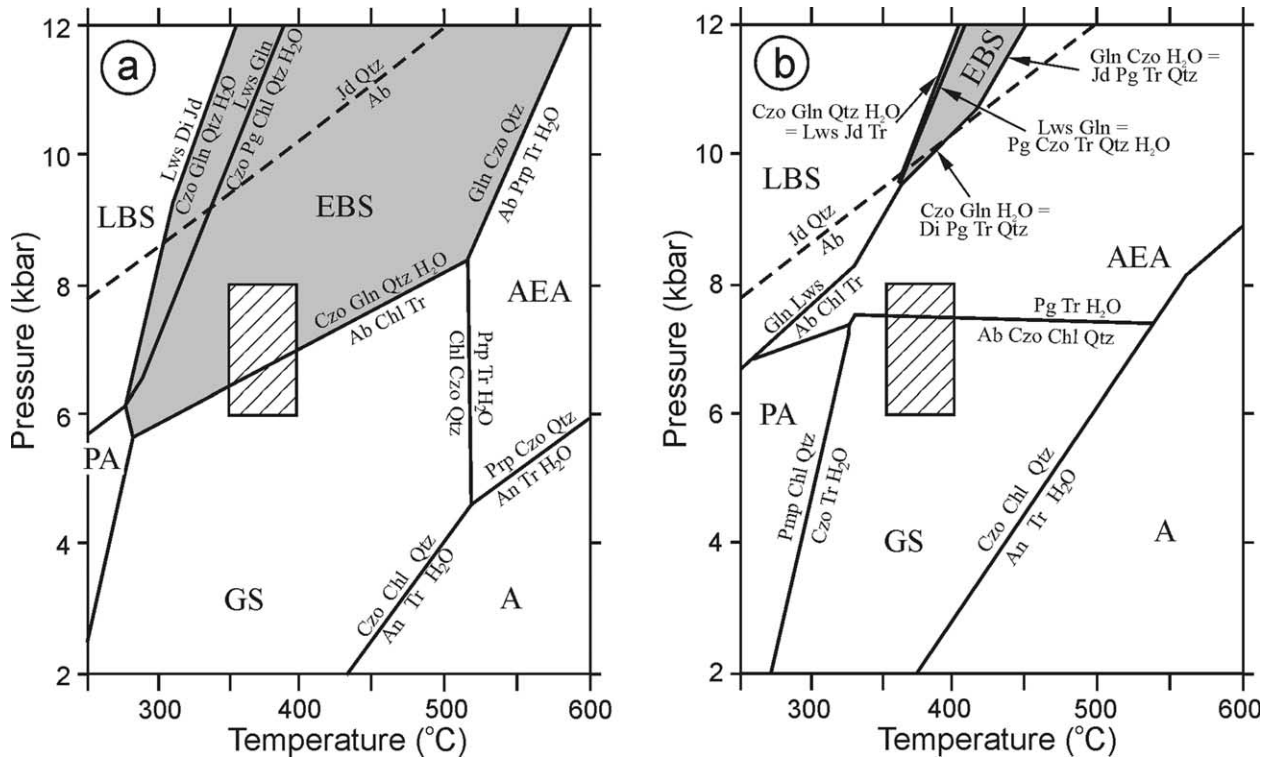

Fig. 5. $P–T$ diagrams calculated by Evans (1990) for mafic rocks depending on activities of phases or phase-components. (a) ferrous compositions, (b) magnesian compositions. EBS = epidote-blueschist paragenesis (grey); LBS = lawsonite-blueschist paragenesis, AEA = albite–epidote–amphibolite paragenesis, A = amphibolite paragenesis, GS = greenschist paragenesis, PA = pumpellyite–actinolite facies paragenesis. Shaded rectangles show positions of blueschist (a) and greenschist (b) from the Terekta Complex. Glaucophane is stable in Fe-rich rocks, while actinolite is stable in Mg-rich rocks.

occurs in Fe-rich rocks, while actinolite develops in Mg-rich rocks. Experimental data suggest also that glaucophane is stabilized by Fe at lower $P–T$ conditions (Maruyama et al., 1986). Thus, glaucophane can develop in some rocks, whereas actinolite can be stable in other rocks at the same $P–T$ conditions due to differences in bulk-rock chemistry, or, in other words, the studied greenschists have potentially recrystallised at the same $P–T$ conditions as the blueschists.

5. Discussion

The presence of metabasalts with geochemical features typical of ocean island basalts and MORB in the Terekta Complex, as well as layered Mn-rich metacherts, marbles, metagraywackes, and adjacent ophiolite plates (serpentinites, sepentinized dunites and pyroxenites) indicates that the complex was a subduction-accretionary complex, containing fragments of deformed oceanic crust and rocks of accretionary wedge. The complex is comparable in protolith compositions with accretionary complexes of active continental margins of the Cordillerian type (Maruyama et al., 1996).

As a whole, the Terekta Complex bears a resemblance to the combination of the Sanbagawa blueschist belt and the Mikabu greenschist belt in Japan (Wallis and Banno, 1990), which are lateral equivalents but differ in metamorphic grade and structural level. Metabasites of the Sanbagawa belt also comprise alkali basalts with relict pyroxene. By contrast, the Mikabu greenschist complex is composed of tholeiite basalts, turbidites, volcaniclastic rocks, and Mn-rich metacherts. Serpentinite blocks are also found within the Sanbagawa belt. The main distinction between the Terekta Complex and the Sanbagawa belt is the lower metamorphic grade of the Uimon blueschists (oligoclase–biotite zone is absent here). The close lithological similarity of these high-pressure/low-temperature complexes allows us to conclude that the Terekta Complex is a constituent of an ancient accretionary prism in Gorny Altai.

The protolith rocks of the Terekta Complex are likely to originate at the early stage of development of the orogenic system and represent the beginning of the Altaid evolution in Late Proterozoic. We believe that the tectonic juxtaposition of the different lithologies took place before their metamorphism, i.e. before subduction or within the subduction zone. The metamorphic age is approximately dated as Upper Ordovician–Early Silurian (Buslov, 1998). But recent imbricated structure of the terrane incorporating high grade metamorphic rocks, unmetamorphosed sediments, and ophiolite plates along with the Terekta rocks is a result of ‘oblique’ collision of the Altai-Mongolian terrain and the Siberian Craton (Buslov et al., 2000). The collision has culminated in Devonian dextral strike-slip faulting in this area (Buslov et al., 2000; Buslov et al., 2001).

Does the occurrence of blueschists indicate a subduction of Paleo-Asian Ocean in Gorny Altai? If the ophiolite melange occurring in the northern part of the metamorphic terrane has originated within a back-arc basin, then the presence of the HP/LT rocks probably only indicate a collision and closure event of back-arc small ocean basin. This problem is still debatable.

Acknowledgements

We thank E.N. Nigmatulina for microprobe analyses, and all the participants of the Third Workshop IGCP-420 for fruitful discussion. Our grateful thanks go to B.-M. Jahn, J.G. Liou and M. Ballèvre for critical and constructive reviews of the manuscript. Financial support was given by the Russian Fund for Fundamental Research (N 02-05-64622 and N 00-05-65203).

References

Buslov, M.M., 1998. Terrain tectonics and geodynamics of folded regions of the mosaic-block type (on the example of the Altai-Sayan and East Kazakhstan regions), Dr Science Thesis, United Institute of Geology, Geophysics and Mineralogy, Novosibirsk, Russia

Buslov, M.M., Watanabe, T., 1996. Intrasubduction collision and its role in the evolution of an accretionary wedge: the Kurai zone of Gorny Altai (Central Asia). Russian Geology and Geophysics 37, 74–84.

Buslov, M.M., Fujiwara, Y., Safonova, I.Yu., Okada, Sh., Semakov, N.N., 2000. The junction zone of the Gorny Altai and Rudny Altai terrains: structure and evolution. Russian Geology and Geophysics 41, 383–397.

Buslov, M.M., Saphonova, I.Yu., Watanabe, T., Obut, O.T., Fujiwara, Y., Iwata, K., Semakov, N.N., Sugai, Y., Smirnova, L.V., Kasansky, A.Yu., 2001. Evolution of the Paleo-Asian Ocean (Altai-Sayan Region, Central Asia) and collision of possible Gondwana-derived terranes with the southern marginal part of the siberian continent. Journal of Asian Earth Sciences 3, 203–224.

Currie, K.L., Van Staal, C.R., 1999. The assemblage stilpnomelane-chlorite-phengitic mica: a geothermobarometer for blueschist and associated greenschist terranes. Journal of Metamorphic Geology 17, 613–620.

Dobretsov, N.L., Lepezin, G.G., Pukinskaya, O.S., 1972. Blueschists in the Altai-Sayan folded region. Doklady AN SSSR 206, 200–203 (in Russian).

Dobretsov, N.L., Buslov, M.M., Simonov, V.A., 1991. Accociated ophiolites, blueschists and eclogites in Gorny Altai. Doklady AN SSSR 318, 413–417 (in Russian).

Duk, G.G., 1982. Higher-pressure greenschist belts (Gorny Altai), Nauka, Leningrad, 184 p (in Russian).

Duk, G.G., 1995. Blueschist, blueschist/greenschist and ophiolite complexes of the Uralian–Mongolian Folded Belt, St Peterburg, 272 p (in Russian).

El-Shazly, A.E.K., 1994. Petrology of lawsonite–pumpellyite, and sodic amphibole-bearing metabasites from north-east Oman. Journal of Metamorphic Geology 12, 23–48.

Evans, B.W., 1990. Phase relations of epidote-blueschists. Lithos 25, 3–23.

Jahn, B.M., Wu, F.Y., Chen, B., 2000. Massive granitoid generation in Central Asia: Nd isotope evidence and implication for continental growth in the Phanerozoic. Episodes 23, 82–92.

Holland, T.J.B., Powell, R., 1998. An internally consistent thermodynamic data set for phases of petrological interest. Journal of Metamorphic Geology 16, 309–343.

Kovalenko, V.I., Yarmolyuk, V.V., Kovach, V.P., Kotov, A.B., Kazakov, I.K., Salnikova, E.B., 1996. Sources of Phanerozoic granitoids in Central Asia: Sm–Nd isotope data. Geokhimiya 8, 699–712 (in Russian).

Kuznetsova, L.G., 1985. Factual description of blueschist complexes in the USSR. Novosibirsk, P.H. IGG SB AN SSSR, 156 (in Russian).

Leake, B.E., Wooley, A.R., Alps, C.E.S., Birch, W.D., Gilbert, M.C., Grice, J.D., Hawthorne, F.C., Kato, A., Kish, H.J., Krivovichev, V.G., Linthout, K., Laird, K., Mandarino, J.A., Maresch, W.V., Nickel, E.H., Rock, N.M.S., Schumacher, J.C., Smith, D.C., Stephenson, N.C.N., Ungaretti, L., Whittaker, E.J.W., Youzhi, G., 1997. Nomenclature of amphiboles: report of the Subcommittee on amphiboles of the International Mineralogical Association, Commision on new minerals and mineral names. Canadian Mineralogist 35, 219–246.

Maruyama, S., Suzuki, K., Liou, J.G., 1983. Greenschist–amphibolite transition equilibria at low pressures. Journal of Petrology 24, 583–604.

Maruyama, S., Cho, M., Liou, J.G., 1986. Experimental investigations of blueschist–greenschist transition equilibria: pressure dependence of Al_2O_3 contents in sodic amphiboles—a new geobarometer. In: Evans, B.W., Brown, E.H. (Eds.), Blueschists and eclogites: Geological Society of America Memoir, vol. 164., pp. 1–6.

Maruyama, S., Liou, J.G., Terabayshi, M., 1996. Blueschists and eclogites of the world and their exhumation. International Geological Review 38, 485–594.

Meschede, M., 1986. A method of discriminating between different types of mid-ocean ridge basalts and continental tholeiites with the Nb–Zr–Y diagram. Chemical Geology 56, 207–218.

Plotnikov, A.V., Kruk, N.N., Vladimirov, A.G., Kovach, V.P., Zhuravlev, D.Z., Moroz, E.N., 2003. Sm–Nd isotope systematics of metamorphic rocks in the Western Altai-Sayan Folded Belt. Doklady Earth Sciences 388, 63–67.

Sengör, B.M.A., Natal'in, B.A., Burtman, V.S., 1993. Evolution of the Altaid tectonic collage and Palaeozoic crustal growth in Eurasia. Nature 364, 299–307.

Triboulet, C., 1992. The (Na–Ca) amphibole–albite–chlorite–epidote–quartz geothermobarometer in the system S–A–F–M–C–Na–H_2O. 1. An empirical calibration. Journal of Metamorphic Geology 10, 545–556.

Wallis, S., Banno, S., 1990. The Sambagawa belt—trends in research. Journal of Metamorphic Geology 8, 393–399.

Winkler, H.G.F., 1976. Petrogenesis of metamorphic rocks, Springer, New York, 348 p.